# Diffuse Scattering and Phason Fluctuations in the Zn-Mg-Sc Icosahedral Quasicrystal and Its Zn-Sc Periodic Approximant

M. de Boissieu,[1,*] S. Francoual,[1,2] Y. Kaneko,[3] and T. Ishimasa[3]

[1]*Laboratoire de Thermodynamique et de Physico-Chimie Métallurgique, UMR CNRS 5614, ENSEEG-INPG, BP 75, 3 8402 Saint Martin d'Hères, France*

[2]*Institut Laue Langevin, BP 156, 38042 Grenoble Cedex 9, France*

[3]*Research Group of Material Physics, Graduate School of Engineering, Hokkaido University, Kita-ku, Sapporo, 060-8628, Japan*

(Received 19 April 2005; revised manuscript received 21 July 2005; published 2 September 2005)

We report on the absolute scale measurement of the x-ray diffuse scattering in the ZnMgSc icosahedral quasicrystal and its periodic approximant. Whereas the diffuse scattering in the approximant is purely accounted for by thermal diffuse scattering, an additional signal is observed in the quasicrystal. It is related to phason fluctuations as indicated by its $Q_{\mathrm{per}}^2$ dependence. Moreover, when compared to previous measurements carried out on the *i*-AlPdMn phase, we find that the amount of diffuse scattering is smaller in the *i*-ZnMgSc phase, in agreement with larger phason elastic constants in this phase. This is confirmed by the observation of a large number of weak Bragg peaks having a high $Q_{\mathrm{per}}$ reciprocal space component.

DOI: 10.1103/PhysRevLett.95.105503 PACS numbers: 61.44.Br, 61.10.Eq

Quasicrystals (QC) are long range ordered materials with a symmetry incompatible with translation invariance [1]. Their diffraction pattern exhibits sharp Bragg reflections, with, for instance, fivefold symmetry in the case of icosahedral phases [see Ref. [2] for an introduction]. As for any aperiodic crystals, [3], the long range aperiodic order brings new Goldstones modes, named phason modes. Their origin is better understood in the high dimensional description of aperiodic crystals, where the periodicity is restored.

For icosahedral quasicrystals, the structure can be embedded in a six-dimensional (6D) space which decomposes in two orthogonal 3D subspaces: the physical (parallel) and the perpendicular (complementary) space. The periodic 6D lattice is decorated with 3D atomic surfaces. The 3D quasicrystalline structure is obtained as a section of the 6D decorated lattice by the parallel space. The invariance of the system free energy under a uniform translation of the cut space along the perpendicular space brings three phason modes which are predicted to be collective diffusive excitations [4,5].

Most of the experimental work in QC systems has been carried out in the *i*-AlPdMn phase, where phason modes have been evidenced using diffuse scattering measurements analyzed in the framework of the hydrodynamic elasticity theory of quasicrystals [6–8]. The temperature dependence of the diffuse scattering has been interpreted as the result of pretransitional phason fluctuations, frozen in below 500 °C because of kinetic reasons [9], while activated above. The diffusive character of long-wavelength phason dynamics has been recently evidenced using coherent x-ray photon correlation spectroscopy [10].

The hydrodynamic theory is a continuum theory, which does not give a microscopic description of phason modes. Whereas the microscopic interpretation of phason modes is well understood in a few incommensurately displacive modulated phases, where damped propagative phason modes have been observed [11], this is still an open problem for QC. Because of the specific geometry of QC structures, when a phason mode fluctuation sets in the system, it results in correlated atom exchanges or ''atom flip'' between double-well sites having similar local environments, but too close to be occupied simultaneously. Modeling of this situation has been mostly carried out for the 3D Penrose random tiling, where tiles are allowed to reshuffle. In this model system, phason modes are hydrodynamics in agreement with theoretical predictions. The ''restoring force'' described by the phason elastic constants is related to the configurational entropy of the system which is maximal in the quasicrystal [12]. However, modeling real atomic structure is not yet achieved, and the physics of phason modes at the atomic scale in QC remains an open question.

To gain some insight into the microscopic of phason modes we present a comparative study of the diffuse scattering measured on an absolute scale in both the ZnMgSc icosahedral phase [isostructural to the *i*-CdYb quasicrystal [13]] and the $Zn_{85}Sc_{15}$ periodic approximant (cubic phase, Im3 space group, $a = 1.384$ nm) [14]. Both the periodic approximant and the quasicrystal share similar local environments. The same atomic cluster is found in both phases, and is packed on a bcc lattice in the approximant and quasiperiodically in the QC [15]. Indeed, the structure of the approximant can be generated from the 6D representation of the QC by tilting the cut space until it reaches a rational slope. As a result, the crystal and the quasicrystal have similar local ''atom flip'' configurations. Despite these similarities in the local order, we show, in the following, that diffuse scattering due to phason modes only shows up in the QC.

Single grains of the $Zn_{85}Sc_{15}$ cubic and $Zn_{80.5}Mg_{4.2}Sc_{15.3}$ icosahedral phases were obtained by slow cooling from the liquid state, annealed at 650 and 750 °C, respectively, and subsequently quenched in water [14]. In order to avoid surface damage by polishing, we

 

used fractured single grain samples. This led to approximately flat surfaces, with a size of $3 \times 3$ mm$^2$ for both phases.

Measurements of the diffuse scattering have been carried out on the D2AM beam line located on a bending magnet at the European Synchrotron Radiation Facility. The incoming x-ray energy was selected by a double Si111 monochromator and set to 9.3 keV, to avoid Zn fluorescence. To minimize parasitic scattering, samples were placed under an evacuated Be hemisphere, and measurements carried out in reflection geometry. The measured diffuse scattering intensity has been set on an absolute scale (e.u./Å$^3$, where e.u. stands for electron unit) using an Al powder sample for flux calibration and after correction from sample absorption. The absolute scale diffuse scattering is proportional to the differential scattering cross section of the sample, for one volume unit, allowing for a comparative study of the amount of diffuse scattering intensity between various samples [16].

The intensity distribution of strong Bragg reflections is similar in the approximant and the quasicrystal. Although Bragg reflections lie on a periodic lattice for the approximant, they display a pseudoicosahedral symmetry. In fact, a phason strain matrix allows us to map indices of the quasicrystal Bragg peaks onto the ones of the approximant.

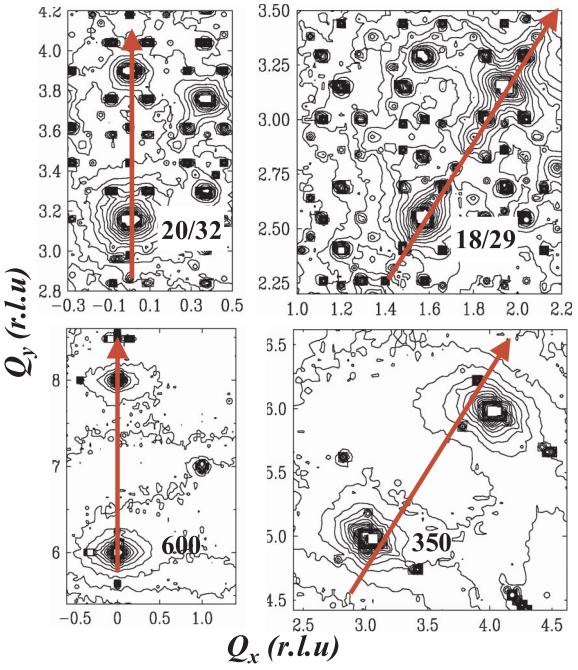


FIG. 1 (color online). Isointensity contours of the diffuse scattering measured in two identical portions of the reciprocal space for the ZnSc periodic approximant (bottom) and the ZnMgSc icosahedral phase (top). Arrows indicate the twofold (left) and fivefold (right) high-symmetry axes. The scattering plane is twofold. Axes coordinates are expressed in $2\pi/a_{6D}$ and $2\pi/a$ units (or reciprocal space unit, r.l.u.) for the quasicrystal and the approximant, respectively.

For instance, the strong 18/29 fivefold axis reflection in the quasicrystal [where we have used the $N$ and $M$ indices following [17] ] corresponds to the (3 5 0) reflection. This is illustrated on Fig. 1 which displays isointensity contours of the scattered intensity measured in two similar areas of the reciprocal space for the approximant (bottom) and the quasicrystal (top). Arrows indicate the twofold (left) and fivefold (right) high-symmetry axes. As visible on the figure the number of Bragg reflections is much larger in the $i$-ZnMgSc phase.

The shape anisotropy of the diffuse scattering is also very different in both phases. In the periodic approximant, the diffuse scattering shape is identical around all Bragg reflections: it has the form of an ellipsoid elongated along the direction transverse to the **Q** vector. This is what is expected for the contribution from thermal vibrations in an almost isotropic solid. The situation is quite different in the quasicrystal, where the shape anisotropy of the diffuse scattering located around Bragg reflections is changing from one Bragg peak to the other.

A more quantitative and detailed analysis has been carried out by considering $Q$ scans performed around selected Bragg peaks and along directions parallel to high-symmetry axis. The shape and the intensity distribution of the diffuse scattering have been analyzed in the framework of the hydrodynamic theory of crystals and quasicrystals. For the icosahedral phase, the diffuse scat-

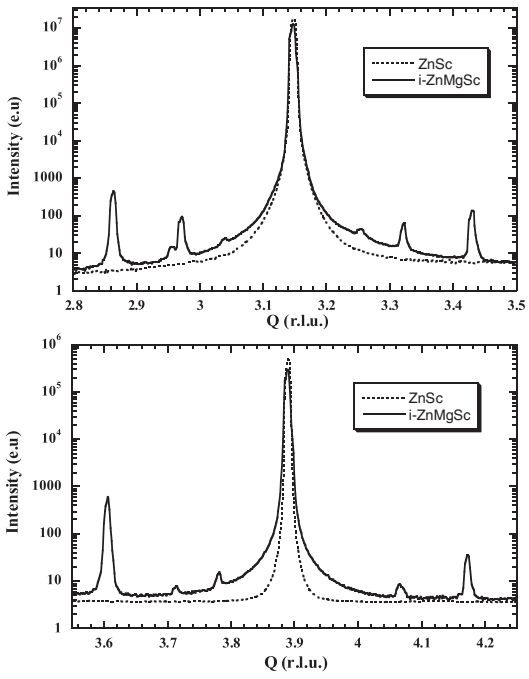


FIG. 2. Comparison of the diffuse scattering intensity on an absolute scale in the ZnSc approximant and the ZnMgSc quasicrystal, for two twofold reflections having different values of their $Q_{per}$ component. Top: (6 0 0) and 20/32 reflections; bottom: (8 0 0) and 32/48. The intensity of the (8 0 0) reflection has been renormalized to the one of the 32/48 reflection.

tering intensity depends on 5 elastic constants: the two Lamé coefficients $\lambda$, $\mu$, the two phason elastic constant $K1$ and $K2$, and a phonon-phason coupling term $K3$. Each 6D reciprocal lattice vector $\mathbf{Q}$ decomposes in two 3D orthogonal components: $\mathbf{Q}_{\mathrm{par}}$, the physical, observable reciprocal vector and $\mathbf{Q}_{\mathrm{per}}$, the complementary component. In the case where the $K3$ coupling term can be neglected, the diffuse intensity $S(\mathbf{Q}_{\mathrm{par}} + \mathbf{q})$ measured at a distance $\mathbf{q}$ from a Bragg peak includes both a phonon and a phason part given by [8]:

$$S(\mathbf{Q}_{\mathrm{par}} + \mathbf{q}) = I_{\mathrm{Br}} q^{-2} (\alpha Q_{\mathrm{par}}^2 + \beta Q_{\mathrm{per}}^2), \qquad (1)$$

where $I_{\mathrm{Br}}$ is the Bragg peak intensity. $\alpha$ and $\beta$ are given by the eigenvalues of the inverse of the hydrodynamic matrix. They depend on the $\mathbf{q}$ direction and on the Lamé and phason elastic constants, respectively. The $\alpha Q_{\mathrm{par}}^2$ term in Eq. (1) corresponds to the thermal (phonon) diffuse scattering (TDS) and is the only term contributing to the signal in the case of the crystal.

Since the sound velocities and thus Lamé coefficients are almost identical in the crystal and the QC [18], there should be a $Q_{\mathrm{per}}$ dependent supplementary contribution in the QC if phason modes take place. This is indeed the case, as illustrated in Fig. 2, which compares the intensity distribution around two Bragg reflections in both the crystal and the quasicrystal. The amount of diffuse scattering is larger in the quasicrystal than in the crystal. Moreover, the relative excess diffuse scattering is larger for the 32/48 reflection (bottom) whose $Q_{\mathrm{per}}$ component is larger than the 20/32 one (top).

From the absolute scale measurements it is possible to extract values of the elastic constants in both the crystal and the QC. For this purpose the $q^{-2}$ decay of the diffuse intensity [Eq. (1)] around various reflections has been fitted as $\mathrm{m}q^{-2}$, from which $m$ is extracted. Since the diffuse intensity is proportional to $I_{\mathrm{Br}}$, the pertinent parameter to consider and reported hereafter is $m/I_{\mathrm{Br}}$, equal to $(\alpha Q_{\mathrm{par}}^2 + \beta Q_{\mathrm{per}}^2)$ [Eq. (1)].

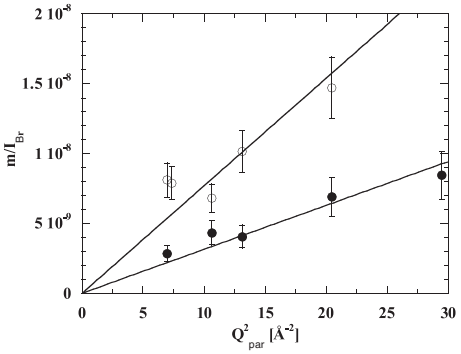


FIG. 3. Evolution of $m/I_{\mathrm{Br}}$ as a function of $Q^2$ for the cubic approximant. Open and full circles stand for transverse and longitudinal scans. The longitudinal and transverse sound velocities are extracted from the two linear fits.

In the case of the crystal, when $\mathbf{q}$ is parallel (longitudinal) or perpendicular (transverse) to $\mathbf{Q}$, the Eq. (1) leads to $m/I_{\mathrm{Br}} = Q_{\mathrm{par}}^2 k_B T / V_{T(L)}^2$, where $V_T$ and $V_L$ stand for the transverse and longitudinal sound velocities, respectively. Since $V_T$ is smaller than $V_L$, this results in an ellipsoidal shape of the diffuse intensity, which one is elongated in the transverse direction, as observed experimentally on Fig. 1. Sound velocities are extracted from the linear variation of $m/I_{\mathrm{Br}}$ with $Q_{\mathrm{par}}^2$ as shown on Fig. 3. We find sound velocities $V_T$ and $V_L$ equal to $2370 \pm 150$ and $4040 \pm 300$ $\mathrm{ms}^{-1}$, respectively, in good agreement with the ones obtained by inelastic x-ray and neutron scattering ($2510 \pm 50$ and $4850 \pm 100$ $\mathrm{ms}^{-1}$) [18]. This thus confirms that the observed diffuse scattering in the approximant mainly originates from thermal vibrations.

In the case of the QC both the TDS and phason terms contribute to the signal and to the fitted value $\mathrm{m}/I_{\mathrm{Br}}$. Since sound velocities and densities are almost equal in the approximant and the QC, the TDS contribution can be easily evaluated and subtracted by computing the quantity $\mathrm{m}/I_{\mathrm{Br}} - \alpha Q_{\mathrm{par}}^2$ [Eq. (1)]. When plotted as a function of $Q_{\mathrm{per}}^2$ (Fig. 4), there is a linear trend which demonstrates that the origin of the supplementary contribution to the diffuse scattering signal is indeed related to phason modes. On this figure, we have reported on the same graph results obtained for twofold and fivefold reflections and different direction of the wave vector $\mathbf{q}$ in reasonable agreement with the weak anisotropy of the diffuse scattering.

Assuming that $K3$ can be neglected, phason elastic constants can be evaluated and are found to be of the order of $K1/k_B T = 0.5 \pm 0.2$ $\mathrm{atom}^{-1}$ and $K2/K1 = -0.15 \pm 0.1$. It has to be noticed that the observed shape anisotropy and intensity distribution of the diffuse scattering is not completely reproduced by these values, as can be seen by the scattered distribution of points in Fig. 4. Including the $K3$ phonon-phason coupling term does not improve much

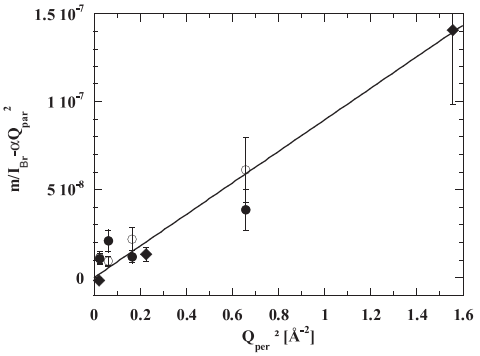


FIG. 4. Evolution of $m/I_{\mathrm{Br}}$ corrected for the phonon contribution as a function of $Q_{\mathrm{per}}^2$, for scans performed along a single direction $q$ centered on reflections on a single high-symmetry axis. Full and open circles stand for transverse and longitudinal $q$ scans around twofold Bragg peaks. Diamonds stand for transverse $q$ scans around fivefold reflections. The solid line is a guide for the eyes.

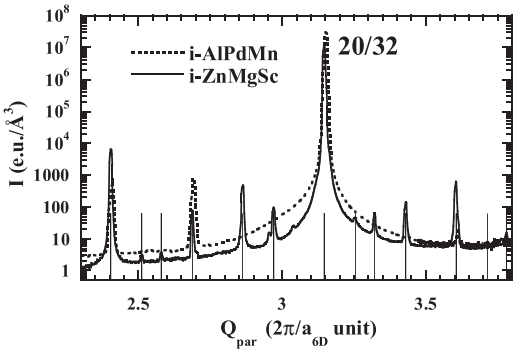


FIG. 5. Comparison of the diffuse intensity, measured on an absolute scale in the *i*-AlPdMn (dashed line) and the *i*-ZnMgSc icosahedral phase (solid line) along a twofold axis. The *i*-AlPdMn data have been renormalized with respect to the Bragg intensity of the 20/32 reflection of the *i*-ZnMgY one. Vertical bars on the $Q$ axis indicate the theoretical position of Bragg reflections with a $Q_{\mathrm{per}}$ component up to 8 r.l.u..

the agreement. This indicates that the observed diffuse scattering may also contain a contribution different from a pure hydrodynamic one.

It is interesting to compare the present results with the one obtained in the *i*-AlPdMn phase, for which $K1/k_BT = 0.1$ atom$^{-1}$, $K2/K1 = -0.53$ at room temperature [7]. The $K1$ value is thus larger in the *i*-ZnMgSc than in the *i*-AlPdMn phase. Since the diffuse scattering intensity roughly scales with $1/K1$, there should be a smaller diffuse scattering intensity in the *i*-ZnMgSc. This is indeed what is observed experimentally as shown in Fig. 5, where both absolute scale data are presented: the amount of diffuse scattering is 3 to 4 times smaller in the *i*-ZnMgSc phase.

As a result, the perpendicular (phason) Debye-Waller factor $B_{\mathrm{per}}$, proportional to the mean squared perpendicular ''fluctuations'' of the atomic surfaces, and which also roughly scales with $1/K1$, is much smaller in the *i*-ZnMgSc than in the *i*-AlPdMn phase. This has important consequences on the diffraction pattern, visible on Fig. 5. Indeed a large number of weak reflections, having a large $Q_{\mathrm{per}}$ component, are visible for the *i*-ZnMgSc phase, whereas they are absent in the *i*-AlPdMn one [19]. In fact, this twofold diffraction pattern can only be indexed by considering very ''high $Q_{\mathrm{per}}$'' reflections with values up to 8 (in $2\pi/a_{6\mathrm{D}}$ units) (vertical bars on Fig. 5), to be compared with 2.5 in the case of the *i*-AlPdMn phase, where the larger perpendicular Debye-Waller factor suppresses high $Q_{\mathrm{per}}$ reflections.

The present results thus show that phason elastic constants depend on the system, as already inferred from the *i*-AlCuFe and *i*-AlPdRe studies [20]. The details of the chemical interactions certainly play a crucial role in that respect. Nevertheless, it also demonstrates that the local order is not sufficient to set in long-wavelength phason modes, since they are not observed in the periodic approximant. The quasiperiodic long range order is indeed necessary for phason modes to show up.

In conclusion, we have shown that whereas the diffuse scattering of the ZnSc approximant is only due to thermal vibrations, a supplementary contribution, related to phason modes, is observed in the *i*-ZnMgSc quasicrystal. This demonstrates that long-wavelength phason modes are indeed a characteristic of the quasiperiodic long range order. The $K1$ phason elastic constant is found to be larger in the *i*-ZnMgSc than in the *i*-AlPdMn quasicrystal. As a result, we observe both a smaller amount of diffuse scattering and a larger number of weak Bragg peak in the *i*-ZnMgSc phase.

We thank J. F Berar and N. Boudet for their help in setting up the experiment on the D2AM beam line.

*Electronic address: boissieu@ltpcm.inpg.fr

[1] D. Shechtman, I. Blech, D. Gratias, and J. W. Cahn, Phys. Rev. Lett. **53**, 1951 (1984).
[2] C. Janot, *Quasicrystals: A Primer* (Oxford University, New York, 1992).
[3] T. Janssen, O. Radulescu, and A. N. Rubtsov, Eur. Phys. J. B **29**, 85 (2002).
[4] P. A. Kalugin, A. Y. Kitayev, and L. S. Levitov, J. Phys. (Paris), Lett. **46**, L601 (1985); P. Bak, Phys. Rev. Lett. **54**, 1517 (1985); D. Levine *et al.*, Phys. Rev. Lett. **54**, 1520 (1985).
[5] T. C. Lubensky, S. Ramaswamy, and J. Toner, Phys. Rev. B **32**, 7444 (1985).
[6] M. de Boissieu *et al.*, Phys. Rev. Lett. **75**, 89 (1995).
[7] A. Létoublon *et al.*, Philos. Mag. Lett. **81**, 273 (2001).
[8] M. V. Jaric and D. R. Nelson, Phys. Rev. B **37**, 4458 (1988); Y. Ishii, Phys. Rev. B **45**, 5228 (1992); M. Widom, Philos. Mag. Lett. **64**, 297 (1991).
[9] M. Boudard *et al.*, Europhys. Lett. **33**, 199 (1996).
[10] S. Francoual *et al.*, Phys. Rev. Lett. **91**, 225501 (2003).
[11] R. Currat and T. Janssen, Solid State Phys. **41**, 201 (1988).
[12] C. L. Henley, in *Quasicrystals: The State of the Art*, edited by D. P. DiVicenzo and P. Steinhardt (World Scientific, Singapore, 1991), p. 429.
[13] A. P. Tsai *et al.*, Nature (London) **408**, 537 (2000).
[14] Y. Kaneko *et al.*, Philos. Mag. Lett. **81**, 777 (2001); Jpn. J. Appl. Phys. **41**, L1112 (2002).
[15] H. Takakura *et al.*, Philos. Mag. Lett. **81**, 411 (2001).
[16] *Diffuse X-ray Reflections from Crystals*, edited by W. A. Wooster (Dover, New York, 1997).
[17] J. W. Cahn, D. Shechtman, and D. Gratias, J. Mater. Res. **1**, 13 (1986).
[18] S. Francoual *et al.* (to be published).
[19] Note that the density of Bragg peaks also depends on the shape of the atomic surfaces describing the structure. A larger atomic surface will produce a much faster decay of the intensity as a function of $Q_{\mathrm{per}}$ than a smaller one.
[20] M. Boudard *et al.*, Mater. Sci. Eng. A **294-296**, 217 (2000); M. de Boissieu *et al.*, J. Alloys Compd. **342**, 265 (2002).